

Nucleation and triggering of earthquake slip: effect of periodic stresses

JAMES H. DIETERICH

U.S. Geological Survey, 345 Middlefield Road, M.S. 977, Menlo Park, CA 94025 (U.S.A.)

(Received January 28, 1986; revised version accepted July 4, 1986)

Abstract

Dieterich, J.H., 1987. Nucleation and triggering of earthquake slip: effect of periodic stresses. In: R.L. Wesson (Editor), *Mechanics of Earthquake Faulting*. *Tectonophysics*, 144: 127–139.

Results of stability analyses for spring and slider systems, with state variable constitutive properties, are applied to slip on embedded fault patches. Unstable slip may nucleate only if the slipping patch exceeds some minimum size. Subsequent to the onset of instability the earthquake slip may propagate well beyond the patch. It is proposed that the seismicity of a volume of the earth's crust is determined by the distribution of initial conditions on the population of fault patches that nucleate earthquake slip, and the loading history acting upon the volume. Patches with constitutive properties inferred from laboratory experiments are characterized by an interval of self-driven accelerating slip prior to instability, if initial stress exceeds a minimum threshold. This delayed instability of the patches provides an explanation for the occurrence of aftershocks and foreshocks including decay of earthquake rates by time⁻¹. A population of patches subjected to loading with a periodic component results in periodic variation of the rate of occurrence of instabilities. The change of the rate of seismicity for a sinusoidal load is proportional to the amplitude of the periodic stress component and inversely proportional to both the normal stress acting on the fault patches and the constitutive parameter, A_1 , that controls the direct velocity dependence of fault slip. Values of A_1 representative of laboratory experiments indicate that in a homogeneous crust, correlation of earthquake rates with earth tides should not be detectable at normal stresses in excess of about 8 MPa. Correlation of earthquakes with tides at higher normal stresses can be explained if there exist inhomogeneities that locally amplify the magnitude of the tidal stresses. Such amplification might occur near magma chambers or other soft inclusions in the crust and possibly near the ends of creeping fault segments if the creep or afterslip rates vary in response to tides. Observations of seismicity rate variations associated with seasonal fluctuations of reservoir levels appear to be consistent with the model.

Introduction

This study applies a previously described model for the nucleation of the earthquake instability (Dieterich, 1986) to questions related to the triggering of earthquakes by periodic loads such as earth tides or loads arising from cyclic filling and draining of reservoirs. This model is based directly on laboratory observations of fault constitutive properties. Of specific interest is the possible role fault constitutive properties have in controlling the degree of correlation between seismicity rates and periodic loads. Other aspects of fault interac-

tions are not treated or have been considerably simplified.

In the previous study (Dieterich, 1986) the incorporation of velocity- and state-dependent constitutive properties (as observed in laboratory experiments) into a model for the nucleation of unstable slip was found to introduce a delay between the time the applied stress reached a critical state and the time of the resulting unstable slip event. Additionally, it is found the fault is capable of temporarily sustaining a load in excess of the minimum stress required to nucleate an instability. In that study it was proposed that mainshocks

following foreshocks and aftershocks result from this type of delayed instability following stress steps associated with the prior earthquakes. Results presented below for the nucleation of earthquake slip in the presence of a periodic loading component indicate that the poor correlation of seismicity rates with earth tides can be explained by observed state- and velocity-dependent constitutive properties. Additionally, if values for constitutive parameters measured in the laboratory are representative of faults in nature, then the poor correlation between tides and earthquakes may be indicative of the stress level acting on faults in nature.

Nucleation patch model

The model for the nucleation of earthquake slip initiating on an embedded fault patch has been outlined previously (Dieterich, 1986). Here we briefly review the nucleation patch model and the fault constitutive properties it employs. Additional discussion of the model and applications to the scaling of premonitory fault creep and to foreshock and aftershock sequences are given by Dieterich (1986). The fault constitutive properties are based directly on laboratory experiments which have demonstrated ubiquitous velocity-, time-, and displacement-dependence of fault strength. These properties are well-represented by state variable constitutive laws. Experimental results and characteristics of the constitutive law are discussed in detail by Dieterich (1979, 1981), Rice (1983), Ruina (1983, 1985), Weeks and Tullis (1985), and Okubo and Dieterich (1986).

Displacement-dependent effects in experiments and in the constitutive law used to model the initiation of unstable fault slip scale by a characteristic slip distance, D_c . Throughout this paper fault displacements, d , and slip velocity, v , are normalized by the characteristic slip distance and are indicated by capitalized letters:

$$D = d/D_c \quad V = v/D_c \quad (1)$$

We represent fault strength as a coefficient of friction, μ , defined by:

$$\mu = \tau/\sigma \quad (2)$$

where τ is the shear stress acting across the fault

and σ is the normal stress. Throughout, σ is considered to be constant during slip. The constitutive law for μ is:

$$\mu = \mu_0 + B_1 \ln[B_2\theta + 1] - A_1 \ln[(A_2/V) + 1] \quad (3)$$

where μ_0 , A_1 , A_2 , B_1 , and B_2 are experimentally determined parameters, V is the normalized slip speed and θ is the state variable that depends on slip history. It is noted that eqn. (3) is equivalent to that of Dieterich (1979, 1981) with the distinction that the earlier forms employ somewhat awkward quotients that are well represented by eqn. (3). At V and θ well removed from the rate limits (i.e., $B_2\theta \gg 1$, $A_2/V \gg 1$), eqn. (3) is exactly equivalent to that employed by Ruina (1980, 1983) and later by several other investigators.

Sliding history effects and consequently displacement- and time-dependent effects are represented by the variable θ which has been interpreted (Dieterich, 1979; Dieterich and Conrad, 1984) as the average age of the load supporting contacts between the sliding surfaces. Because contacts are destroyed and created during slip, θ depends on the slip history. The following law for the evolution of θ has been discussed by Ruina (1980) and employed by Dieterich (1981, 1986):

$$d\theta/dt = 1 - \theta V \quad (4)$$

From eqn. (4) note that for a locked fault $V = 0$, $d\theta/dt = 1$ and consequently the change of θ is equal to elapsed time. Because the large and rapid displacements of an earthquake will reset θ to values approaching zero, a fault that has remained locked since the previous earthquake will have θ approximately equal to the time interval from the earthquake. In the simulations discussed below, values of θ are associated with the interevent times of earthquakes and values in the range from 10^7 to 10^{10} s are employed.

It is useful to define two special cases of eqn. (3) for discussion of slip instability. Under steady state conditions, $d\theta/dt = 0$ and $V = 1/\theta$, which yields from eqn. (3) the steady state friction μ_s :

$$\mu_s = \mu_0 + B_1 \ln(B_2/V + 1) - A_1 \ln(A_2/V + 1) \quad (5a)$$

or equivalently:

$$\mu_s = \mu_0 + B_1 \ln(B_2\theta + 1) - A_1 \ln(A_2\theta + 1) \quad (5b)$$

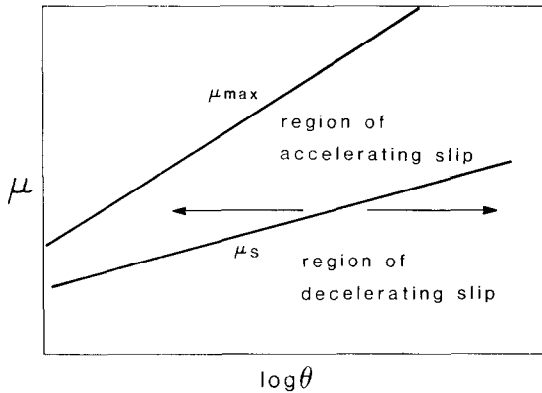


Fig. 1. Plot of maximum friction, μ_{\max} , and steady state friction, μ_s , against the state variable θ . Under conditions of constant stress, μ , slip speed and θ will remain constant only at $\mu = \mu_s$. Under conditions of $\mu > \mu_s$ and constant stress, slip speed will accelerate and θ will decrease with time. When $\mu = \mu_{\max}$ instability occurs. The stress range $\mu_{\max} > \mu > \mu_s$ defines the conditions under which self-driven accelerating slip ending in instability may occur. At $\mu < \mu_s$, under conditions of constant stress, slip speed decreases and θ increases. The arrows indicate the direction in which θ evolves at stresses not at μ_s .

Under sliding conditions where $B_2/V \gg 1$ and $A_2/V \gg 1$ in eqn. (5a) the contribution of the summation with 1 in the logarithmic terms becomes negligible and eqn. (5a) may be written as:

$$\mu_s = \mu'_0 + (A_1 - B_1) \ln V \quad (6a)$$

where:

$$\mu'_0 = \mu_0 + B_1 \ln B_2 - A_1 \ln A_2 \quad (6b)$$

This eqn. (6a) is the form given by Ruina (1980, 1983) and employed by several others for the velocity dependence of the steady state friction. The maximum limit of frictional strength, μ_{\max} , occurs when $V \gg A_2$ with the result that eqn. (3) becomes:

$$\mu_{\max} = \mu_0 + B_1 \log(B_2\theta + 1) \quad (7)$$

At stresses (i.e., $\mu = \tau/\sigma$) between μ_s and μ_{\max} , fault slip speed is greater than the steady state speed. As μ approaches μ_{\max} , V approaches infinity. In the quasi-static analysis employed below, instability occurs at the instant the applied stress reaches the limiting strength μ_{\max} . The process by which μ reaches μ_{\max} inevitably involves decreasing μ_{\max} because accelerating slip results in evolution of θ to smaller values. Dieterich (1979, 1986),

Koslov and Liu (1980), and Gu et al. (1984) show that self-driven acceleration of slip to instability, without additional externally driven loading, can occur in the range $\mu_{\max} > \mu > \mu_s$. See Fig. 1.

Results of stability analyses for spring and slider systems with these constitutive properties, when applied to slip on faults embedded in an elastic medium, show that unstable slip may initiate only on fault patches that exceed some critical size (Dieterich, 1986). Slip on patches less than the critical size is always stable. For a circular patch the critical patch radius, r_c , is approximately:

$$r_c = \frac{7\pi G D_c}{24\sigma\xi} \quad (8)$$

where G is the shear modulus and ξ is a parameter obtained from spring-slider stability criteria. The results of Ruina (1980, 1983) and Rice and Ruina (1983) for the critical stiffness for instability from perturbation of slip at $\mu = \mu_s$ yield $\xi = (B_1 - A_1)$. For sliding above the steady state friction ($\mu > \mu_s$) the Ruina and Rice value for ξ is a lower bound. The previous study (Dieterich, 1986) shows that slip instability can arise on a patch of fixed size and that patch size only weakly affects the slip history as long as $r > r_c$. Slip history is controlled by the constitutive properties.

The previous results lead to a central notion of the approach presented here: conditions on the fault patch where the instability originates control the timing of the earthquake instability. It is proposed that within a seismically active volume of the earth's crust there exist a population of potential nucleation patches. Characteristics of the distribution of conditions on the population of fault patches where earthquake slip nucleates and the loading history determine the details of occurrence rates of earthquakes originating within the volume. Subsequent to the onset of the earthquake instability within the nucleating patch, the instability may propagate well beyond the patch. Processes associated with rupture propagation, not addressed by this model, control the size of the earthquake.

For the sake of simplicity it is assumed that the nucleating fault patch is embedded in a homogeneous elastic medium, adjoining portions of the fault are locked prior to the onset of the instabil-

ity, and physical properties and slip conditions on the center of the patch are sufficient to characterize the problem. Under these assumptions the equations governing slip on the patch are identical to those governing a simple spring and slider system. Possible interactions between nearby patches are not treated.

For the computational results presented below, the model for a nucleation patch is represented as a single slider attached to spring with a constant stiffness. The fault obeys the constitutive law (3) and the evolution law of eqn. (4). The computations employ normalized displacements and velocity for the fault, D and V , respectively. Velocity of the load point attached to the spring V_L is also normalized by D_c . Stress acting perpendicular to the sliding surface, σ , is constant during slip permitting the shear stress acting on the surface and fault frictional strength to be normalized by σ . Because the analysis is for quasi-static motions, the applied stress equals the friction at all times. The normalized shear stress, μ' , acting on the patch is:

$$\mu' = \mu + K(V_L t - D) + S \sin(t/P) \quad (9)$$

At $t = 0$, $D = 0$, and $\mu = \mu'$. Note that the periodic loading component is treated here as a simple sinusoid. K is the normalized patch stiffness:

$$K = 7\pi G D_c / 24 \sigma r \quad (10)$$

The radius of the patches employed for the computations described below is expressed as a factor of the critical radius for steady state sliding, r_c .

To follow the evolution of slip on the patch, the computations employ a time marching procedure to find slip velocity. Slip is treated as a series of constant velocity time steps. The solution for the unknown slip velocity during each time step satisfies the condition that the average frictional resistance equals the average stress applied by the spring during the time step. The average friction and applied stress during the step are obtained by numerical integration. The evolution of θ during the time step is given by the constant velocity solution of eqn. (4):

$$\theta = 1/V + (\theta_0 - 1/V) e^{-D} \quad (11)$$

where $\theta = \theta_0$ at $D = 0$. Use of eqn. (11) has been found to satisfactorily represent evolution of θ

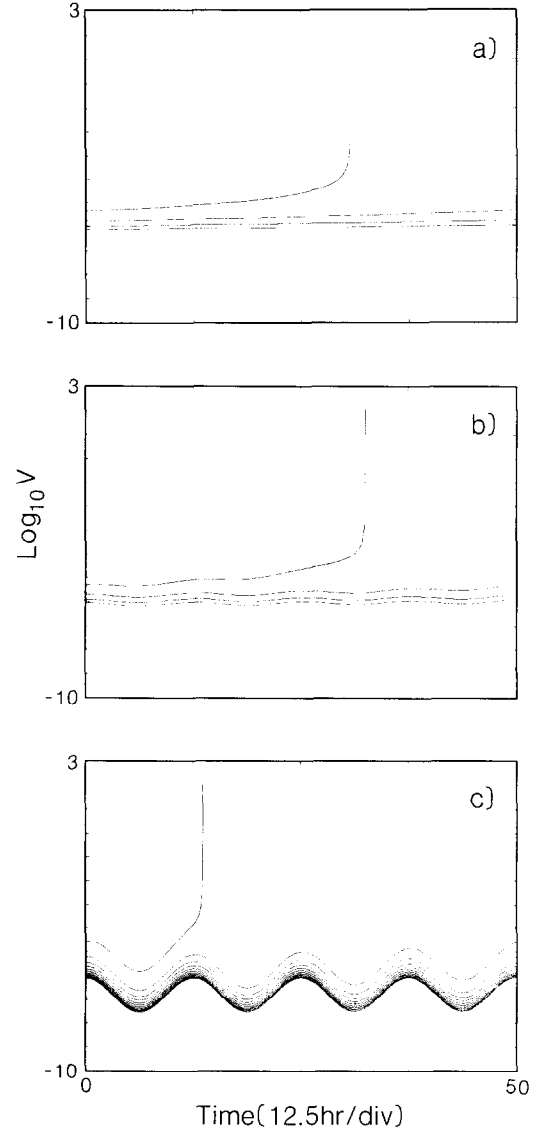


Fig. 2. Slip speed plotted against time from numerical computations in which the amplitude of the periodic loading component, S , was 5×10^{-5} , 5×10^{-4} , and 5×10^{-3} for a, b, and c, respectively. Note that the amplitude of the slip speed variations caused by S may be obtained directly from eqn. (3). The constitutive parameters are $A_1 = 0.003$, $A_2 = 1.0$, $B_1 = 0.006$, and $B_2 = 1.0$.

under conditions of varying slip rate subject to the conditions that small displacement steps are employed and that the change in slip rate between steps is sufficiently small. The computational approach employed maximum displacement steps of $0.04D$ with a maximum change of slip rate $\Delta V/V = 0.05$. Use of smaller steps did not alter the

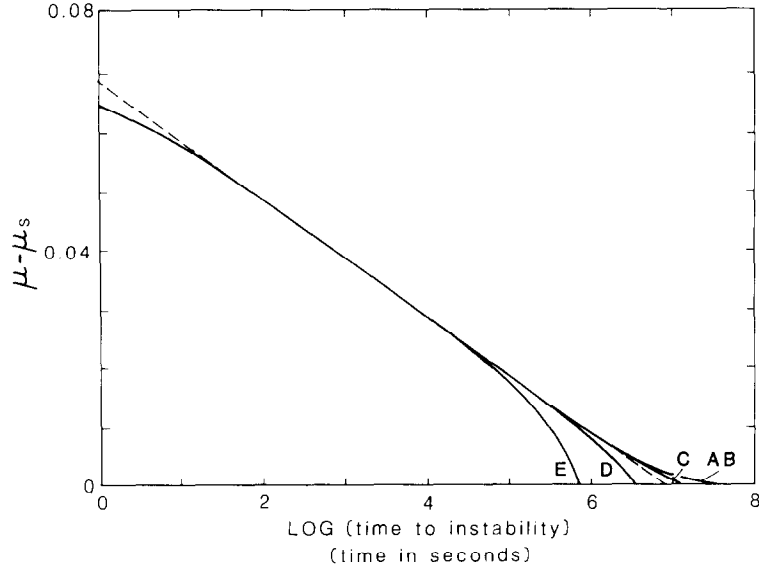


Fig. 3. Delayed instability following application of initial stress $(\mu - \mu_s)_0$ for different loading point velocities. The constitutive parameters were chosen to be representative of the experimental results: $B_1 = 0.015/2.3$, $A_1 = 0.010/2.3$, and $A_2 = 1.0$. At the time the initial stress is applied $\theta = 10^7$ s. The radius $r = 10r_c$. Loading point velocities are $V_L = 0, 10^{-7}, 10^{-6}, 10^{-5}$, and 10^{-4} for the curves labeled A, B, C, D, and E, respectively. The broken line is the fit to the solution by eqn. (3). From Dieterich (1986).

results. An instability occurs whenever the applied stress exceeds μ_{\max} .

Figure 2 illustrates the results for slip velocity as a function of time for different amplitudes of the periodic loading component S . The period for this example is 12.5 hrs. Note that the logarithm of the instantaneous slip velocity prior to rapid acceleration is proportional to amplitude of the periodic stress, S , and to the constitutive parameter A_1 .

The time to nucleate unstable slip in the absence of a periodic load is given by Fig. 3. The figure gives the times to instability, t , following the application of an initial stress in the range $\mu_{\max} > \mu > \mu_s$. Each curve was obtained from a series of numerical computations for the time to instability using different initial stresses and with fixed patch radius, constitutive parameters and initial θ . The different curves give the results for different loading rates, V_L . Note that the logarithm of the time to instability shows a linear dependence upon the initial stress over a wide range of times. Similar results are obtained when the patch stiffness (radius) was varied. The time to instability decreases slightly as the patch radius increases. The difference in the logarithm (base

10) of the times to instability for the limiting cases of $r = r_c$ and $r = \infty$ is given by Dieterich (1986) to be about 0.2. These results and results from computations where r , θ , and the constitutive parameters were systematically varied all showed a linear dependence of initial stress and the logarithm of the time to instability over a large range of times. In this interval, the results can be fit to the following empirical equation:

$$(\mu - \mu_s)_0 = C + A_1 \ln(\theta_0/t) \quad (12)$$

where C is a constant depending in part upon r . In eqn. (12) the quantity $(\mu - \mu_s)_0$ is the initial difference between the applied stress and steady state friction and θ_0 is the initial value of the state variable. The broken line in Fig. 3 is a plot of eqn. (12). This fit to the numerical results provides a very good representation of the time to instability during the final stages of the process of accelerating slip in the range of conditions where $\mu > \mu_s$ and the accelerating slip rates on the patch dominate over the loading of the patch by V_L . The departure of the numerical solutions for t from eqn. (12) as μ approaches μ_{\max} is only a few seconds which for the purpose of this study is considered to be negligible when compared to

seismic interevent times or the loading periods employed. In the absence of externally driven loading, as the initial stress difference is decreased to zero, the numerical solutions for the time to instability diverge from the empirical fit and apparently go to infinity. For finite loading rates the times to instability are all finite. Note in Fig. 3 that for a long interval of time prior to the instability, eqn. (12) provides an excellent representation of the numerical results and that the results are independent of the loading conditions.

Population distributions and seismicity rates

We consider now the distribution of conditions for a population of nucleation patches within a volume of interest and the seismicity rates that would result from a loading history acting on the population. The following assumes that the constitutive parameters (A_1 , A_2 , B_1 , B_2 , and D_c), the patch radius and the loading history are the same everywhere in the volume. The quantities that vary over the population of patches are θ and the applied stress μ , which also vary as a function of time and patch slip as required by eqns. (4) and (9). The approach followed is to first establish the characteristics of the distribution of θ and μ that will yield constant rates of seismicity under conditions of constant loading rate ($V_L = \text{constant}$, $S = 0$). Then, different loading histories are applied to the population to find the effect of the non-constant loading rates on the seismicity rates.

A nucleation patch will creep at accelerating rate as the time of instability approaches. As a result, μ and θ on each patch will evolve as the slip accelerates. However, it is not necessary to completely describe the (μ, θ) path followed by each patch to arrive at some conclusions about the distributions of μ and θ yielding constant seismicity rates.

For those patches at some sufficiently low μ , the slip speed, V , obtained from eqn. (3) will be negligible when compared to the loading rate imposed by V_L . Under those conditions, the patch may be considered locked. For constant rate loading, prior to significant creep, the time to reach some reference stress state $(\mu - \mu_s)_r$ is:

$$(\mu - \mu_s)_r = (\mu - \mu_s)_0 + KV_L t \quad (13)$$

where $(\mu - \mu_s)_0$ is the initial stress on some patch in the population at $t = 0$. For a uniform rate of seismicity, R :

$$N = Rt \quad (14)$$

where N is the number of patches that have nucleated an instability in time t . It is reasonable to assume that each patch follows the same (μ, θ) path, at least in some average sense. It follows then, for there to be constant rate of instability in the volume, the patches must reach not only instability, but any other (μ, θ) point along the path at regular time intervals. Consequently, R is the rate at which the conditions on the patches pass any point in the path, including the arbitrary reference point $(\mu - \mu_s)_r$. For those patches that are locked, combining eqns. (13) and (14) to eliminate t yields the distribution of initial stresses:

$$(\mu - \mu_s)_0 = (\mu - \mu_s)_r - N(KV_L/R) \quad (15)$$

Consequently, prior to the acceleration of slip, the stresses on the nucleation patches, $(\mu - \mu_s)_0$, at time $t = 0$ are uniformly distributed over the population of patches.

Dieterich (1986) proposed that foreshocks and aftershocks arise from delayed instability on nearby nucleation patches following a stress step at the time of the prior earthquake. Specifically, effect of a stress step is to alter the condition of constant loading rate by imposing a step in the applied stress that shifts the stresses acting on the population of eqn. (15) upward by an amount sufficient to cause the self-driven accelerating slip that leads to an earthquake instability. The number of earthquakes with time following a stress step is obtained by combining eqn. (15) with the result for the time to instability (12) which yields:

$$N = \frac{R[(\mu - \mu_s)_r + \Delta\mu - C - A_1 \ln(\theta_0/t)]}{KV_L} \quad (16)$$

where $\Delta\mu$ is the stress step. Differentiating eqn. (16) to obtain rate of instability following the stress step:

$$\frac{dN}{dt} = \frac{A_1 R}{KV_L t} \quad (17)$$

Equation (17) yields the familiar $1/t$ decay in aftershock rates and the similar statistical relation-

ship found for the times of occurrence for fore-shock–mainshock pairs reported by Jones and Molnar (1976, 1979) and Jones (1985).

To evaluate the effects of a periodic loading component it is important to note that the periodic loading perturbation operates continuously up to the instant of failure on each patch. As a result it is necessary to consider the distribution of conditions (θ and μ) up to the time of failure. As patch slip rates accelerate approaching instability, the slip velocity dominates over loading velocity and evolution of θ becomes important. Here we establish some characteristics of the distribution of conditions for a population of patches approaching instability that will yield a constant rate of instability occurrence in the absence of a periodic load. Below, populations of patches having these properties are subjected to a shear stress with a periodic component. From the result of eqn. (12) the time to failure, t , may be expressed as:

$$t = \psi \exp(C/A_1) \quad (18)$$

where the parameter ψ is defined as:

$$\psi = \theta_0 / \exp[(\mu - \mu_s)_0 / A_1] \quad (19)$$

In eqn. (18) note that the time to failure is now given in terms of a single variable for the conditions on the nucleation patch. Combining eqn. (18) with eqn. (14) yields the distribution of ψ for a population of patches that produces a constant rate of seismicity in the absence of loading perturbations:

$$\psi = \psi_0 [(N/Rt_0) + 1] \quad (20)$$

This uses the definition from eqn. (18) that:

$$\exp(C/A_1) = t_0 / \psi_0$$

Results for periodic loading

The numerical computations for time to instability with a periodic loading component employ the procedures previously outlined. A series of separate computations were made using different initial values for μ and θ that satisfy the distribution of eqn. (20). The time interval separating successive instabilities in the population yields the seismicity rate for that interval. Note

that although the single parameter, ψ , is sufficient to describe the distribution of conditions of the population needed to yield constant instability rates in the stress range where accelerating creep dominates, additional information is needed to fully describe the individual distributions of θ_0 and μ . Two end-member cases have been examined. With the first, the initial θ_0 on all patches was taken to be the same, and $(\mu - \mu_s)_0$ was adjusted to satisfy eqn. (20). The second case fixed the initial $(\mu - \mu_s)_0$ the same everywhere and adjusted θ_0 to satisfy eqn. (20). The former case is quite artificial in that it is difficult to envision a situation in nature that would yield a population with these characteristics. The latter distribution, however, approximates that required for a population of patches having a very large radius compared to the critical radius.

Each of the end-member cases yields constant time intervals between successive instabilities when the amplitude of the periodic load, S , is set equal to zero. When a periodic component is added to the loading condition, the time intervals become nonuniform. The results are identical for both distributions indicating that the parameter ψ is fully sufficient to describe those characteristics of the population that control the time to instability under different loading conditions.

Figure 4 gives the results from a series of calculations with loading at a 12.5-hr period to simulate the dominant component of the solid earth tide. Each simulation utilizes a different value for the amplitude S of the periodic load. For the series of simulations illustrated, the stiffness and loading velocity are zero and the constitutive parameters are: $A_1 = 0.003$, $A_2 = 1.0$, $B_1 = 0.006$, $B_2 = 1.0$. The figure plots instability rate in the population as a function of time in the loading period. The instability rate is normalized by the average rate, R , over the 12.5-h period. Note that the maximum and minimum rates occur at the time of the maximum and minimum in the periodic signal. For the purpose of discussing these results the maximum change of instability rates over the loading cycle, R_a , is defined as follows:

$$R_a = (R_{\max} - R_{\min}) / R \quad (21)$$

where R_{\max} and R_{\min} are the maximum and

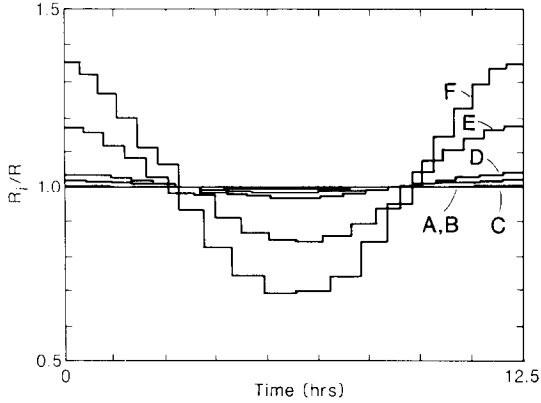


Fig. 4. Rates of instability occurrence for a population of nucleation patches acted upon by a 12.5-hr periodic load with amplitude $S = 0, 1 \times 10^{-5}, 5 \times 10^{-5}, 1 \times 10^{-4}, 5 \times 10^{-4},$ and 1×10^{-3} for the curves labeled A, B, C, D, E, and F, respectively. R_i/R is the rate of occurrence of instabilities divided by the average rate, R , over the 12.5-hr period of the cyclic load. Constitutive parameters are $A_1 = 0.003, A_2 = 1.0, B_1 = 0.006,$ and $B_2 = 1.0$.

minimum rates, respectively, and R is the average rate.

Rates of instability occurrence using a number

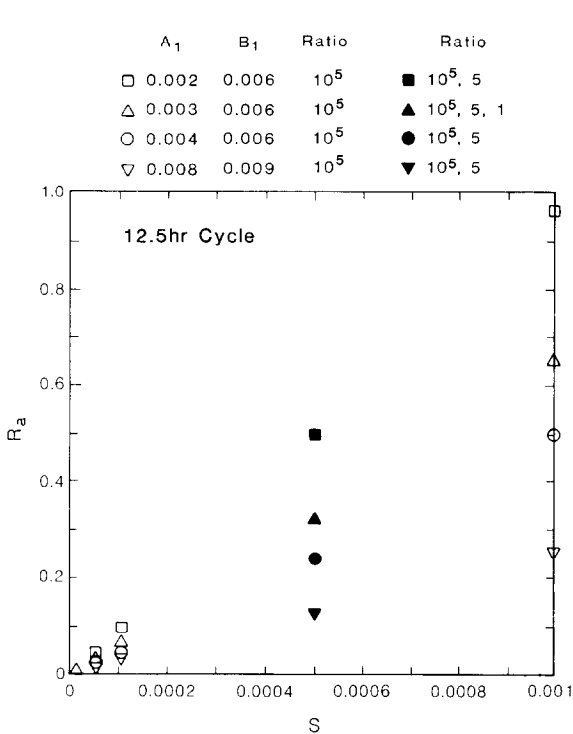


Fig. 5. Change of instability rate, $(R_{\max} - R_{\min})/R$, as a function of amplitude S for 12.5-hr periodic load. Legend gives the constitutive parameters and patch radius. The results are insensitive to $A_2, B_1,$ and B_2 .

of different constitutive parameters, amplitudes, S , and crack radius were studied. All simulations yielded results for the variation of rates with time that were qualitatively similar to the above example. Figure 5 summarizes these results for R_a as a function of amplitude S .

Several features of these results are of interest: (1) stiffness (patch radius) and loading velocity have no effect on R_a ; (2) at the resolution of the computations, there is no discernable shift of R_{\max} and R_{\min} with respect to the maximum and minimum in the periodic loading component of the fault stress; (3) for a fixed set of constitutive parameters, the rate difference, R_a , is proportional to the amplitude of the periodic loading amplitude, S ; (4) the magnitude of R_a is not affected by the constitutive parameter B_1 but varies inversely with the constitutive parameter A_1 .

These results suggest the simple scaling law for R_a :

$$R_a = 2S/A_1 \tag{22}$$

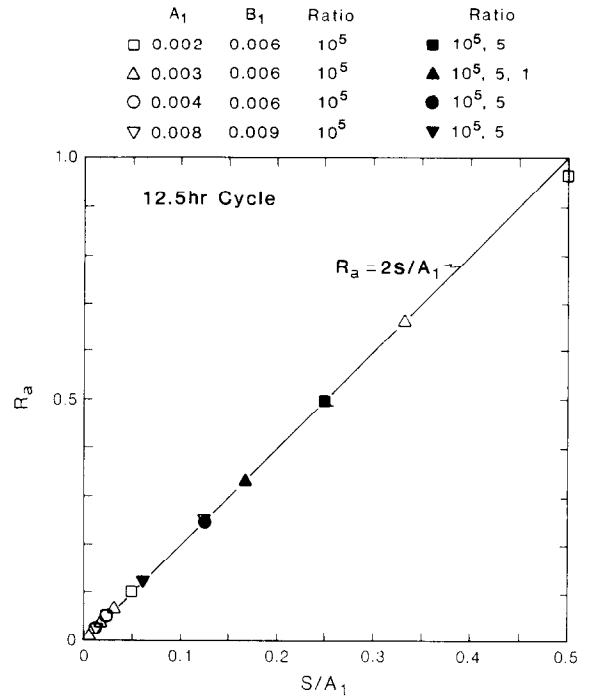


Fig. 6. Change of instability rate $(R_{\max} - R_{\min})/R$, for 12.5-hr periodic load. Data are those of Fig. 5. In this case the data are plotted against S normalized by A_1 . Equation (22) is plotted as the solid line. Legend gives the constitutive parameters and patch radius.

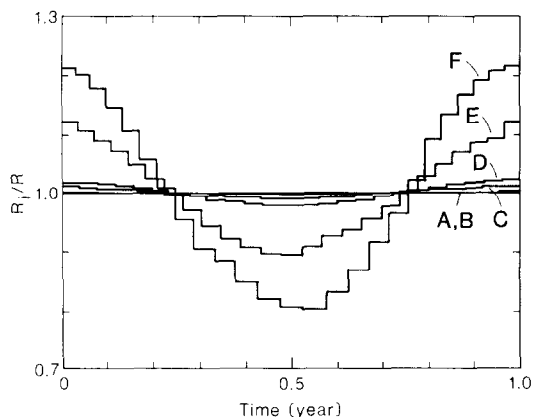


Fig. 7. Rates of instability occurrence for a population of nucleation patches acted upon by a 1-yr periodic load with amplitude $S = 0, 1 \times 10^{-5}, 5 \times 10^{-5}, 1 \times 10^{-4}, 5 \times 10^{-4},$ and 1×10^{-3} for the curves labeled A, B, C, D, E, and F, respectively. R_1/R is the rate of occurrence of instabilities divided by the average rate, R , over the 1-yr period of the cyclic load.

Figure 6 shows the data of Fig. 5 replotted for R_a against S/A_1 . Equation (22) is plotted as the solid line. The deviation of the numerical results from eqn. (22) appears to be well within the apparent accuracy of the numerical computations.

Similar computations were performed using a cyclic loading component with a 1-yr period. The

purpose of these computations was to test for a possible dependence of the result of eqn. (22) on loading period by using a period very different from 12.5-hr. Additionally, an annual cycle could be of interest for earthquakes induced by reservoir loading because reservoirs commonly show a significant seasonal fluctuation of water level.

Figure 7 shows results for instability rate as a function of S , the amplitude of the periodic load and time in the annual cycle. Figure 8 is a summary of all computations with a 1-yr period and plots R_a , the amplitude of the instability rate variation, against S/A_1 . The results for R_a using an annual cycle are the same as those obtained for a 12.5-hr period; they are well represented by eqn. (22) for $S/A_1 < 1.0$. For $S/A_1 > 1.0$, R_a begins to diverge from the empirical relation of eqn. (22).

Discussion and summary

The model presented here utilizes constitutive properties for earthquake faults inferred directly from laboratory experiments. Because of displacement scaling in the constitutive law by the parameter D_c , instabilities on embedded faults can nucleate only if slip occurs on a fault patch with a

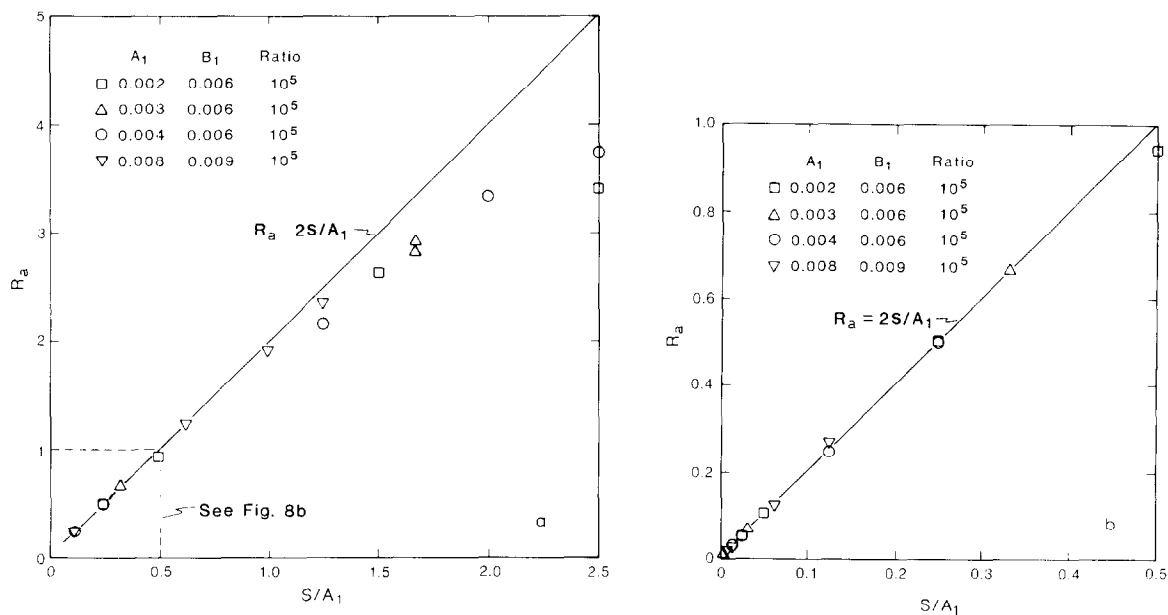


Fig. 8. Change of instability rate, $(R_{\max} - R_{\min})/R$, for a 1-yr periodic load. Summary of all data plotted against S normalized by A_1 . Equation (22) is plotted as the solid line. Legend gives the constitutive parameters and patch radius.

minimum radius, r_c , that is proportional to D_c .

The magnitude of D_c appropriate to faults in nature appears to be an open question at this time. In experiments, D_c correlates with fault roughness and varies from a few microns for smooth surfaces without gouge to about $50\ \mu\text{m}$ for roughened surfaces separated by a layer of gouge (Dieterich, 1981). If the values of D_c from laboratory faults are representative of faults in nature, then the critical radius, r_c , for initiating earthquake instability as obtained from eqn. (8) may be quite small. Additionally, it is found that accelerating premonitory displacements in the interval from 10 days to 10 min preceding instability on the nucleation patch are approximately $5D_c$ (Dieterich, 1986). Using the maximum laboratory values of D_c (0.05 mm) with this model indicates that at $\sigma = 100\ \text{MPa}$, then $r_c = 5\ \text{m}$ and premonitory displacements would be approximately 0.25 mm (Dieterich, 1986). Using the maximum laboratory values of D_c (0.05 mm) with this model indicates that at $\sigma = 100\ \text{MPa}$, then $r_c = 5\ \text{m}$ and premonitory displacements would be approximately 0.25 mm (Dieterich, 1986). These results suggest that accelerating premonitory creep in the nucleation zone could be difficult to detect as a precursor unless D_c in nature is much larger than that measured for the laboratory simulated faults. Estimates of fracture energy for large earthquakes are often quite large and indicate D_c may be on the order of several centimeters. However, recent close-in, high-resolution strain observations prior to some moderate earthquakes show no evidence of accelerating strains prior to those earthquakes (Johnston et al., 1987). Those observations put upper limits on D_c in the range 0.9 mm to 200 mm (Dieterich, 1986).

It is noteworthy that the results for the duration of accelerating slip and the time of occurrence of instability (i.e., eqns. 12 and 22) are independent of D_c . Consequently, the current uncertainty for the appropriate values of D_c for faults in nature does not affect the application of the constitutive law to models for earthquake rates and times of occurrence. Additionally, it may be of interest to note that the empirical equations (12) and (22) depend principally on the constitutive parameter A_1 which is the coefficient for the

direct velocity effect. Although the full constitutive equation is quite complex with several parameters, these results for timing of the earthquake instability are controlled by the viscous term A_1 . This parameter is easily observed in experiments and is apparently insensitive to experimental conditions. The net steady state velocity-dependence of fault strength which is determined by the difference ($A_1 - B_1$) in eqn. (6a) does not control the final results.

It is reasoned that it is the processes within the nucleation patch that control the timing of the earthquake instability, but not necessarily the size of the earthquake. Subsequent to the nucleation of the instability the earthquake may propagate well beyond the nucleation patch. The distribution of initial conditions on a population of potential nucleation patches and the history of stresses acting on the volume will determine the seismicity of a region.

Previously it has been shown there is a delay between the time when stress on a patch exceeds the minimum threshold for instability and the time of instability (Dieterich, 1986). During that interval the fault patch undergoes accelerating slip that culminates in the instability. The time delay is governed by the amount the applied stress exceeds the threshold stress and by the constitutive parameter A_1 . This delayed instability provides a plausible explanation of aftershocks and foreshocks. If it is assumed that the population of patches must have a distribution of conditions that yield constant seismicity rates prior to the stress step of the mainshock, then following the mainshock predicted seismicity rates will decay by $1/t$.

In the discussion below, the model results are applied to the triggering of earthquakes by tidal stresses and seasonal fluctuations in reservoir loads. The following considers only the effects of periodic perturbation of shear stress and fault constitutive properties on seismicity rates. Full analysis of these problems would include many factors that cannot be addressed by the model in its current state. Those factors might include variation of the entire stress field with time, not just the shear stress acting on the fault patches; time- and spatially-dependent variation of fluid pressures; and fault patches with various orientations

with respect to the stress field.

Fault constitutive laws that do not have some type of velocity- or time-dependent fault strength have the characteristic that slip on a fault embedded in a simple elastic medium couples instantaneously to the applied driving stress. The commonly employed slip weakening models in which fault strength drops from a peak to residual value have this characteristic. In such cases, slip instability will occur at the instant some threshold stress is reached. If the applied stress is held just below that threshold, an instability will never initiate. Where fault loading consists of a slowly increasing tectonic stress with a superimposed periodic component, it is the successively higher peaks of the periodic component that will advance the fault stress or displacement. Consequently, for simple models of faults with instantaneous instability at a threshold, earthquakes will always be expected to occur near the times the periodic load reaches its maxima. Although some correlation between earthquake rates and earth tides has been reported in the literature (e.g., Klein, 1976), the enhancement of earthquake occurrence rates at any specific time in the tidal cycle is quite weak in the best examples and in most cases statistically meaningful correlations have not been found (Heaton, 1982).

It might be argued that in the earth, multiple interacting faults may result in loss of coherence between tides and fault stresses with a resulting loss of correlation between tides and earthquake occurrence even if the fault follows a simple threshold criterium for instability. However, this argument is not supported by the evidence from strain records. Strainmeter records from seismic active regions show widespread coherence strain signals at tidal frequencies that are in agreement with theoretical tidal strains. Furthermore, the tidal strains are the dominant short-term strain signal. Yet earthquakes, even those from restricted regions with similar fault orientations, do not display the expected correlation with tidal stresses. This suggests that the idea of earthquake instability occurring instantaneously at a minimum critical threshold, although attractive in its simplicity, is probably an oversimplification when applied to questions of earthquake triggering.

When state variable constitutive properties are utilized, under conditions where earthquake slip nucleates in the presence of a periodic loading component, it is found that instability rates are proportional to the magnitude of the amplitude of the periodic loading component and inversely proportional to the constitutive parameter A_1 (eqn. 22). As A_1 is decreased, the enhancement of seismicity rates under conditions of periodic loading increases and appears to go to infinity as $A_1 \rightarrow 0$. It is seen that at $A_1 = 0$, the fault loses its viscous-like behavior, and from the results of eqn. (12), the fault no longer has time-delayed instability. The results of eqn. (22) for nucleation of unstable fault slip suggest some tentative conclusions for earthquakes occurring under conditions of periodic loading.

By definition from eqns. (2) and (9) the parameter S is the amplitude of the periodic variation of shear stress, τ_p , divided by the normal stress. Using this definition, eqn. (22) is rewritten as:

$$\sigma = (2\tau_p)/(A_1 R_a) \quad (23)$$

If we make some assumptions for the parameters on the right side of eqn. (23), the normal stress range where this model predicts earthquakes to correlate with earth tides can be estimated. We assume, somewhat arbitrarily, that the practical threshold of detection for seismicity rate variations in a catalog is $R_a > 0.1$. In laboratory experiments, the parameter A_1 is consistently found to have values in the range 0.003–0.007. Taking $A_1 = 0.005$ and $\tau_p = 0.002$ MPa bar for earth tides we obtain from eqn. (23) that $\sigma < 8$ MPa for there to be observable correlation of earthquakes with tides. This would correspond to depths less than approximately 0.3 km for rocks with no pore fluid pressure, and depths less than about 0.5 km for rocks with pore fluid pressure under normal hydrostatic head. This discussion suggests that the widespread failure to find strong correlation of seismicity with tides can be understood as a direct consequence of the constitutive properties of faults. The parameter A_1 , which controls the immediate velocity-dependent response of fault strength, acts to inhibit correlation of earthquakes with tides. If the value of A_1 for faults in nature is significantly less than that observed for laboratory faults, then

detectable correlation of earthquakes with tidal stresses would be generally expected.

The inverse dependence of R_a on normal stress given by eqn. (23) suggests that examination of earthquake catalogues for tidal correlations using only those earthquakes originating at very shallow depths should produce positive correlations if the normal stresses in the nucleation zones are sufficiently small. In addition, this model implies that correlation with tides could occur at higher normal stresses where inhomogeneities amplify the magnitude of the tidal stress with the result that S is of greater magnitude.

Amplification of tidal stresses could occur near soft inclusions that concentrate the deformation due to tides. Active volcanic regions where subsurface magma reservoirs are undergoing distortion by earth tides are likely candidates for this type of tidal amplification. In this circumstance, the distortion of the reservoir due to the tides could induce stresses adjacent to the reservoir that are significantly greater than the tidal stresses in a homogeneous elastic medium. It is noted that Klein (1976) reports cases of tidal correlation of earthquakes for oceanic rift zones which he attributes to possible enhancement of tidal stress by weakened lithosphere.

Another situation where tidal stresses could possibly be amplified sufficiently to cause detectable seismicity rate changes at high normal stress is in zones adjacent to creeping faults. In this situation stress redistribution arising from fault creep tends to be highly concentrated near the end of the slipping zone. Small changes in slip rate can result in large changes in rate of stress increase. If the slip rate on a creeping fault varies because of the tides, then earthquakes originating near the ends of creep sections could be correlated with tides.

For the case of reservoir loading, seasonal fluctuations of water level obviously may induce complicated stress and pore fluid changes in the vicinity of the reservoir that would require careful case by case treatment to fully understand. However, independent of such complications, strong correlation of reservoir loads and earthquakes are plausible because the amplitude of the stress variation due to reservoir loading can easily be one or

two orders of magnitude larger than the stresses due to earth tides. From eqn. (23) it is seen that this would be expected to result in a proportionate increase of the variation of earthquake rates for reservoirs compared to that for earth tides. For example, if the seasonal fluctuation of water level is 10 m, the reservoir load will vary by 0.1 MPa. If we assume the amplitude of the shear stress change is equal to load change ($\tau_p = 0.05$), then from eqn. (23) we obtain $R_a = 0.8$ and $R_a = 1.3$ at a depth of 1.0 km for the case of fluid pressure equal to zero and normal hydrostatic pressure, respectively. At a depth of 4 km, $R_a = 0.2$ and $R_a = 0.3$ for fluid pressure equal to zero and normal hydrostatic pressure, respectively. These rate changes are of sufficient magnitude to be detected.

References

- Carder, D.S., 1945. Seismic investigations of the Boulder Dam area, 1940–1944, and the influence of reservoir loading on local earthquake activity. *Bull. Seismol. Soc. Am.*, 35: 175–192.
- Chinnery, M.A., 1969. Theoretical fault models. In: K. Kasahara and A.E. Stevens (Editors), *A Symposium on Processes in the Focal Region*. Publ. Dom. Obs., Ottawa, 27(7): 211–223.
- Dieterich, J.H., 1978. Time-dependent friction and the mechanics of stick-slip. *Pure Appl. Geophys.*, 116: 790–806.
- Dieterich, J.H., 1979. Modeling of rock friction: 1. Experimental results and constitutive equations. *J. Geophys. Res.*, 84: 2161–2168.
- Dieterich, J.H., 1981. Constitutive properties of faults with simulated gouge. In: *Mechanical Behavior of Crustal Rocks*. *Geophys. Monogr.*, Am. Geophys. Union, 24: 103–120.
- Dieterich, J.H., 1986. A model for the nucleation of earthquake slip. In: *Earthquake Source Mechanics*. Maurice Ewing Sym. 6. Am. Geophys. Union, Monogr., 37: 37–97.
- Dieterich, J.H. and Conrad, G., 1984. Effect of humidity on time- and velocity-dependent friction. *J. Geophys. Res.*, 89: 4196–4202.
- Gu, J.-C., Rice, J.R., Ruina, A.L. and Tse, S.T., 1984. Slip motion and stability of a single degree of freedom elastic system with rate and state dependent friction. *J. Mech. Phys. Solids*, 32(3): 167–196.
- Guha, S.K., Gosavi, P.D., Agarwal, B.N.P., Padale, J.G. and Marwadi, S.C., 1973. Case histories of some artificial disturbances. *Eng. Geol.*, 8: 59–77.
- Heaton, T.H., 1982. Tidal triggering of earthquakes. *Bull. Seismol. Soc. Am.*, 72: 2181–2200.
- Johnston, M.J.S., Linde, A.T., Gladwin, M.T. and Borchardt, R.A., 1987. Fault failure with moderate earthquakes. *Tectonophysics*, 144 (this issue): 189–206.

- Jones, L.M., 1985. Foreshocks and time-dependent earthquake hazard assessment in southern California. *Bull. Seismol. Soc. Am.*, 75: 1669–1680.
- Jones, L.M. and Molnar, P., 1976. Frequency of foreshocks. *Nature*, 262(5570): 677–679.
- Jones, L.M. and Molnar, P., 1979. Some characteristics of foreshocks and their possible relation to earthquake prediction and premonitory slip. *J. Geophys. Res.*, 84: 5709–5723.
- Klein, F.W., 1976. Earthquake swarms and the semidiurnal solid earth tide. *Geophys. J. R. Astron. Soc.*, 45: 245–295.
- Koslov, D.D. and Liu, H.-P., 1980. Reformulation and discussion of mechanical behavior of the velocity-dependent friction law proposed by Dieterich. *Geophys. Res. Lett.*, 7(11): 913–916.
- Okubo, P.G. and Dieterich, J.H., 1986. State variable fault constitutive relations for dynamic slip. In: *Earthquake Source Mechanics, Maurice Ewing Symp. 6. Am. Geophys. Union, Monogr.*, 37: 25–35.
- Rice, J.R., 1983. Constitutive relations for fault slip and earthquake instabilities. *Pure Appl. Geophys.*, 121: 443–475.
- Rice, J.R. and Gu, J.-C., 1983. Earthquake aftereffects and triggered seismic phenomena. *Pure Appl. Geophys.*, 121(2): 343–349.
- Rice, J.R. and Ruina, A.L., 1983. Stability of steady frictional slipping. *Trans. ASME, J. Appl. Mech.*, 50: 343–349.
- Ruina, A.L., 1980. Friction laws and instabilities: a quasistatic analysis of some dry friction behaviour. Ph.D. Thesis, Brown University, Providence, R.I.
- Ruina, A.L., 1983. Slip instability and state variable friction laws. *J. Geophys. Res.*, 88: 10359–10370.
- Ruina, A.L., 1985. Constitutive laws for frictional slip. In: Z. Bazant (Editor), *Mechanics of Geomaterials*. Wiley, New York, pp. 169–187.
- Simpson, D.W. and Negmatulleaev, S.K., 1981. Induced seismicity at Nurek reservoir, Tadjikistan, USSR. *Bull. Seismol. Soc. Am.*, 71(5): 1561–1586.
- Weeks, J.D. and Tullis, T.E., 1985. Frictional sliding of dolomite: a variation in constitutive behavior. *J. Geophys. Res.*, 90(b9): 7821–7826.